



HAL
open science

High Frame Rate Ultrasound for Electromechanical Wave Imaging to Differentiate Endocardial From Epicardial Myocardial Activation

Francis Bessière, Ali Zorgani, Jade Robert, Loïc Daunizeau, Elodie Cao, Fanny Vaillant, Emma Abell, B. Quesson, Stéphane Catheline, Philippe Chevalier, et al.

► **To cite this version:**

Francis Bessière, Ali Zorgani, Jade Robert, Loïc Daunizeau, Elodie Cao, et al.. High Frame Rate Ultrasound for Electromechanical Wave Imaging to Differentiate Endocardial From Epicardial Myocardial Activation. *Ultrasound in Medicine & Biology*, 2020, 46 (2), pp.405-414. 10.1016/j.ultrasmedbio.2019.10.017 . hal-03033116

HAL Id: hal-03033116

<https://hal.science/hal-03033116>

Submitted on 3 Dec 2020

HAL is a multi-disciplinary open access archive for the deposit and dissemination of scientific research documents, whether they are published or not. The documents may come from teaching and research institutions in France or abroad, or from public or private research centers.

L'archive ouverte pluridisciplinaire **HAL**, est destinée au dépôt et à la diffusion de documents scientifiques de niveau recherche, publiés ou non, émanant des établissements d'enseignement et de recherche français ou étrangers, des laboratoires publics ou privés.

1 **High frame rate ultrasound for electromechanical wave**
2 **imaging to differentiate endocardial from epicardial**
3 **myocardial activation**

4
5 Francis Bessière MD MSc^{1,2,3}, Ali Zorgani PhD^{2,3}, Jade Robert MSc^{2,3}, Loïc Daunizeau
6 MSc^{2,3}, Elodie Cao MSc^{2,3}, Fanny Vaillant PhD^{4,5,6}, Emma Abell MSc^{4,5,6}, Bruno Quesson
7 PhD^{4,5,6}, Stéphane Catheline PhD^{2,3}, Philippe Chevalier MD PhD^{1,3}, Cyril Lafon PhD^{2,3}

8
9 *1- Hôpital cardiologique Louis Pradel, Hospices Civils de Lyon, 69677 Lyon, France*

10 *2- LabTAU, INSERM, Centre Léon Bérard, Université Lyon 1, Univ Lyon, F-69003,*
11 *LYON, France*

12 *3- Université de Lyon, France*

13 *4- IHU Liryc, Electrophysiology and Heart Modeling Institute, fondation Bordeaux*
14 *Université, 33600 Pessac-Bordeaux, France*

15 *5- Université de Bordeaux, Centre de recherche Cardio-Thoracique de Bordeaux,*
16 *U1045, 33000, Bordeaux, France*

17 *6- INSERM, Centre de recherche Cardio-Thoracique de Bordeaux, U1045, 33000*
18 *Bordeaux, France*

19
20
21 None of the authors report any conflict of interest

22

1 Corresponding author:

2 Dr Francis BESSIERE

3 Electrophysiology department, Louis Pradel Cardiovascular Hospital

4 59 boulevard Pinel, 69500 Bron, France

5 E mail : francis.bessiere@chu-lyon.fr

6 Tel : +33472119075

7

8

9

10

11

12

13

14

15

16

17

18

19

20

21

22

23

24

1 **Abstract**

2

3 Differentiation between epicardial and endocardial ventricular activation remains a challenge,
4 despite the latest technologies available. The aim of the present study was to develop a new
5 tool method, based on electromechanical wave imaging (EWI), to improve arrhythmogenic
6 substrate activation analysis. Experiments were conducted on left ventricles (LV) of four
7 isolated working mode swine hearts. The protocol aimed at demonstrating that different
8 patterns of mechanical activation could be observed whether the ventricle was in sinus
9 rhythm, paced from the epicardium, or from the endocardium. Seventy-two EWI acquisitions
10 were recorded on the anterior, lateral, and posterior segments of the LV. Fifty-four loop
11 records were blindly assigned to two readers. EWI sequences interpretations were correct in
12 89% of cases. The overall agreement rate between the two readers was 83%. When in a
13 paced ventricle, the origin of the wave front was focal and originated from the endocardium
14 or the epicardium. In sinus rhythm, wave front was global and activated within the entire
15 endocardium towards the epicardium at a speed of 1.7 ± 0.28 m.s⁻¹. Wave front speeds were
16 respectively measured when the endocardium or the epicardium were paced at a speed of 1.1
17 ± 0.35 m.s⁻¹ vs 1.3 ± 0.34 m.s⁻¹ (p=NS). EWI activation mapping allows activation
18 localization within the LV wall and calculation of the wave front propagation speed through
19 the muscle. In the future, this technology could help localize activation within the LV
20 thickness during complex ablation procedures.

21

22

23 **Keywords:** Electromechanical wave imaging; ventricular arrhythmia; endocardial versus
24 epicardial activation; cardiac mapping; ultrasound

25

1 **Introduction**

2

3 Many options are available to delineate the electrophysiological and anatomical substrates of
4 ventricular arrhythmia, whether it concerns premature ventricular contraction (PVC) or
5 ventricular tachycardia (VT). The electrocardiogram (ECG) is the oldest option. QRS
6 complex duration, polarity, and morphology analysis from a 12-lead surface trace provides
7 clues on the location of the arrhythmia inside the ventricles. However, ECG lacks precision
8 since it is difficult to localize the origin of a *foci* within the thickness of the wall. Such
9 difficulties have already been reported when differentiating endocardial from epicardial
10 VT(Fernandez-Armenta and Berruezo 2014) in the left ventricle (LV), and when attempting
11 to localize PVC in the outflow tract (Lerman 2015)(Enriquez et al. 2017). Recently, high-
12 density extra-cardiac mapping has been developed. A 252-lead surface acquisition merged
13 onto a three dimensional cardiac tomography reconstruction provides real time activation
14 mapping to localize the arrhythmia source (J Shah et al. 2013)(Revishvili et al. 2015)(Erkagic
15 et al. 2015). This promising technology can be used to locate occult paroxysmal arrhythmia
16 during catheter ablation procedures. However, this method is expensive and lacks precision
17 since the body surface acquisition is only able to show the first area activated. In the case of
18 PVC or VT, the system cannot distinguish endocardial from epicardial origin, as the electrical
19 recordings at the surface of the thorax combine information from the entire thickness of the
20 ventricles. A bipolar catheter-based endocardial and epicardial activation mapping system can
21 also be used to more precisely localize the arrhythmia. In such a context, if the underlying
22 electrophysiological mechanism is hyper automatism, it usually allows the localization of a
23 PVC or a VT and when it is a reentrant circuit, the critical isthmus may be determined
24 effectively. However, this technique requires time to yield reliable and useful information to
25 locate and treat the arrhythmia substrate. Sometimes, the exact location of a PVC or VT

1 remains unclear, since it may come from the mid myocardium, or an area that cannot be
2 reached easily by an intra-cardiac catheter (i.e: LV summit)(Enriquez et al. 2017). Moreover,
3 this method remains risky since epicardial access may lead to coronary artery injuries, cardiac
4 perforation, or chronic pericarditis and endocardial access may cause strokes(Shivkumar
5 2019).

6 Ultrasonic quantitative mapping of myocardial activation has been shown to provide global
7 activation maps. High rate recordings from myocardial deformation are gated by the
8 electrocardiogram in such a way that motion can be decomposed while the ECG runs to create
9 the electromechanical wave imaging (EWI). This has been shown to be effective in mapping
10 sinus rhythm activation(Melki et al. 2017) or stimulated rhythm(Bunting et al. 2017)(Costet
11 et al. 2016) in animal models with healthy, infarcted(Costet et al. 2017), or ablated
12 hearts(Papadacci et al. 2017a). More recently, EWI was able to differentiate endocardial from
13 epicardial *foci* (Costet et al. 2018). However, only eight measurements were performed and
14 interpretation was done in a non-blinded manner, preventing a statistically relevant conclusion
15 to be given. In the present preliminary study, experiments were conducted in swine healthy
16 hearts of an isolated working heart model(Vaillant et al. 2016) using local bipolar electrogram
17 signal gated EWI. The aim was to describe local high-resolution endocardial and epicardial
18 activation patterns and characterize wave front propagation within the thickness of the LV
19 wall. Reliability of this method was provided from EWI records of the anterior, lateral, and
20 posterior walls of the LV.

21

22

1 **Materials and Methods**

2 *Animal preparation*

3 The study protocol was approved by the local Animal Research Ethics Committee (CEEA50)
4 in accordance with recommendations of the Directive 2010/63/EU of the European
5 Parliament on the protection of animals used for scientific purposes. Pigs (Large White
6 Landrace, 40 kg, $n = 4$) were pre-medicated with an intramuscular injection of ketamine (20
7 mg/kg), acepromazine (0.1 mg/kg), and buprenorphine (10 $\mu\text{g}/\text{kg}$). Anesthesia was induced
8 with an intravenous bolus of propofol (1 mg/kg) and maintained with ketamine and
9 midazolam (40 $\text{mg}\cdot\text{kg}^{-1}\cdot\text{h}^{-1}$ and 2 $\text{mg}\cdot\text{kg}^{-1}\cdot\text{h}^{-1}$, respectively). Animals were then intubated and
10 ventilated (50/50 air/oxygen), and received an injection of heparin (200 UI/kg).

11 *Excision and perfusion*

12 The swine thorax was opened, and blood was collected (2 L) via the introduction of an 8-Fr
13 sheath into the right jugular vein. Heparin (2500 UI/L) was added in the reservoir to avoid
14 coagulation. Heart was excised according to protocols used in humans during heart
15 transplantation; cardiac arrest was performed in vivo by cross clamping of the ascending aorta
16 and direct injection into the aortic root of 1L of cold (4°C) cardioplegic homemade Custodiol
17 (in mM: NaCl 15, KCl 9, MgCl₂ 4, α -ketoglutaric acid 1, histidine.HCl.H₂O 18, histidine
18 180, tryptophan 2, mannitol 30, CaCl₂ 0.015), before rapid excision and immersion in a cold
19 0.9% saline solution. The aorta, pulmonary artery, pulmonary veins, and superior vena cava
20 were cannulated to perfuse the heart in the isolated working mode. Inferior vena cava vein
21 was sutured to limit leaks.

22 *Isolated heart perfusion in recirculating biventricular-working mode*

1 The chambers used for preload, afterload, and aortic compliance were made from a 1 liter
2 water-jacketed glassware (Radnoti LLC, Monrovia, California, USA) to control the perfusate
3 temperature. Heart reperfusion was performed in the Langendorff mode for 15–20 min to
4 wash out the cardioplegic solution, gradually rewarm the heart and recover a stable ex vivo
5 cardiac function. The Langendorff perfusion pressure was adjusted to achieve 60 mmHg. If
6 necessary, the heart was defibrillated at 10–30 J (Life Pak 12, Medtronic, Minneapolis,
7 Minnesota, USA). The heart was perfused with blood collected on the same animal before
8 heart excision, diluted with a Tyrode buffer (vol/vol: 1/5; in mM: NaCl 128, KCl 4.7, MgCl₂
9 0.7, NaH₂PO₄ 0.5, NaHCO₃ 28, CaCl₂ 1.8, Glucose 11, Pyruvate 0.5, Lactate 1, Mannitol 16).
10 The perfusion medium was gassed with a mix of 95%/5% oxygen for maximal oxygenation
11 and maintained at pH 7.4 and at 37.5°C. A clinical oxygenator and arterial filter (Getinge
12 Group, Rastatt, Bade-Wurtemberg, Germany) were added before the preload reservoir to
13 ensure an optimal oxygenation of the perfusion medium. After stabilization (10 min with
14 spontaneous cardiac rhythm), the system was switched from Langendorff to working mode.
15 Pre- and afterloads were maintained constant during the whole protocol (left atrial pressure:
16 10–15 mmHg; right atrial pressure: 5–10 mmHg; left ventricular afterload: 70–90 mmHg; right
17 ventricular afterload: 15–30 mmHg).

18

19 *Lead placement and pacing protocol*

20

21 Six pacemaker leads (Tendril 52cm, Abbott, Minneapolis, Minnesota, USA) were fixed in
22 pairs, on the anterior, lateral, and posterior walls of the LV. The epicardial leads were
23 attached on the epicardium of the designated portion; under ultrasound guidance endocardial
24 leads were screwed at the exact opposite side of the wall, in such a way that the exact same
25 portion of the LV could be paced from the endocardium or the epicardium. A schematic view

1 and description of the setup is shown in Figures 1 & 2. Each lead was successively connected
2 via a wire to a device controller (Merlin, Abbott, Minneapolis, Minnesota, USA). Pacing
3 parameters were settled 0.2 V above the threshold to get a local capture that would not
4 jeopardize activation mapping within the LV wall. The duration of the stimulus was set at 0.4
5 ms. Sites were consecutively paced 20 bpm above the spontaneous sinus rhythm.

6

7 *Ultrasound acquisition*

8

9 A 15 MHz central frequency ultrasonic probe (L15-Xtech, Vermon, Tours, France) was
10 placed facing the LV wall (Figure 2) and maintained by a hydraulic flexible arm in the same
11 position during the whole experiment. The 2-dimensional probe was connected to an ultrafast
12 ultrasound scanner (Vantage, Verasonics, Kirkland, Washington, USA). Conventional B-
13 mode images were acquired in the short-axis at 50 frames/second to assist myocardial
14 segmentation and to guide the placement of the pacing electrodes. After placing two
15 electrodes at the surface of the heart, a bipolar signal was acquired using an ECG unit (DAM
16 50, Word Precision Instrument, Sarasota, Florida, USA) and recorded using an oscilloscope
17 (PicoScope 3000, Pico Technology, St Neots, UK).

18 An ultrafast imaging sequence was used to acquire 400 B-mode images at a pulse repetition
19 frequency of 2500 frames/second on the first heart (160ms). The last three hearts were
20 recorded using 800 B-mode images acquisition at a pulse repetition frequency of 4000
21 frames/second (200ms), during sinus rhythm, pericardial, or endocardial pacing to maximize
22 the accuracy of the measurements. In order to synchronize the ultrafast acquisition with the
23 bipolar signal wave, an output signal was generated for each frame and superimposed on the
24 bipolar signal. A phase-based motion tracking estimation algorithm(Pinton et al. 2006) was
25 applied to the radiofrequency (RF) data in order to track the electromechanical wave

1 propagation into the LV wall. Unlike speckle tracking algorithm based on RF-Window cross-
2 correlation, this method allows conservation of high spatial resolution of the initial B-mode
3 images.

4

5 *EWI interpretation*

6

7 A total of 4 isolated hearts were analyzed successively. The experiments on the first 2 hearts
8 were carried out to validate the proof of concept. Loops from the anterior wall on the left
9 ventricle were analyzed to describe the scheme of activation when the electrical activation
10 was coming from the epicardium, the endocardium, and in sinus rhythm. Based on the
11 observations from the first 2 hearts, the last 2 hearts were carried out to evaluate the ability of
12 the system to detect the different patterns of mechanical activation when blinded to the
13 electrical activation. Three segments of the LV were successively analyzed: the anterior wall,
14 the lateral wall, and the posterior wall. For every segment and activation mode, EWI loops
15 were recorded three times. Two separate readers (JR and EC) received training based of the
16 observations obtained from the first 2 hearts. Then, blinded to the electrical activation, the
17 same authors qualitatively interpreted the 3-recorded loops of a segment to be in accordance
18 with the predetermined sinus rhythm, endocardial pacing, and epicardial pacing patterns. A
19 sequence of a 3-times recorded loop was considered in accordance when at least 2 of the 3
20 loops were consistent with predetermined patterns. The axial propagation speeds of the wave
21 fronts were computed based on a time of flight method along the thickness of the myocardium
22 wall (i.e. time vs space representation)(Nguyen et al. 2014). Quantitative (mean \pm standard
23 deviation (SD)) and qualitative (%) variables were analyzed. Overall agreement analyses were
24 performed using the Cohen's Kappa index.

25

1 **Results**

2

3 From the first two hearts, 6 EWI sequences were collected and analyzed: 2 in sinus rhythm, 2
4 in epicardial pacing, and 2 in endocardial pacing. EWI sequences were each made by a 3-
5 recordings of the zone (= 18 loops). In sinus rhythm, visual qualitative displays of the wave
6 front scheme were similar between all recordings: the EWI-induced wave front systematically
7 originated from the endocardium and mid myocardium and moved towards the epicardium
8 with a wide and global displacement (Figure 3). During epicardial and endocardial pacing,
9 visual qualitative displays of the wave front demonstrated a focal positive displacement after
10 rising of the local electrical signal. When visible, the origin of the EWI activation matched the
11 location of the epicardial or endocardial leads (Figures 4 and 5).

12

13 From the last two hearts, 18 EWI sequences were collected: 6 in sinus rhythm, 6 in epicardial
14 pacing, and 6 in endocardial pacing. EWI sequences were each made by a 3-recordings of the
15 zone (= 54 loops). Every sequence in sinus rhythm, epicardial pacing, and endocardial pacing
16 were all collected 2 times on the anterior, lateral wall, and posterior walls. Two independent
17 readers analyzed all sequences to provide descriptive statistics (36 lectures = 108 loops
18 analyzed).

19

20 In spontaneous sinus rhythm, the mean \pm SD heart rate was 119 \pm 6bpm; the epicardium and
21 endocardium sides were sequentially paced at a mean \pm SD rate of 138 \pm 9bpm.

22 EWI sequences readings matched the electrical activation in 89% of cases (Table 1). The
23 overall agreement rate between the two readers was 83%.

1 The readers differentiated in 100% of cases, paced from sinus rhythm activations, on the
2 anterior, the lateral, and the posterior walls. Mean±SD propagation speed of the mechanical
3 wave front in sinus rhythm, into the thickness of the muscle, was $1.7\pm 0.28\text{ m}\cdot\text{s}^{-1}$.
4 EWI acquisitions allowed epicardial activation detection in 92% of cases. When on the
5 posterior or anterior walls, activation patterns from the epicardium were analyzed correctly in
6 100% of cases. When on the lateral wall, only 75% of correct analysis was observed (Table
7 1). The mechanical wave front started in a focal zone where the lead was located, and
8 propagated from the epicardium towards the endocardium at a mean±SD speed of 1.3 ± 0.34
9 $\text{m}\cdot\text{s}^{-1}$. EWI acquisitions allowed endocardial activation detection in 75% of cases. When on
10 the posterior wall, activation patterns detected from the endocardial lead were analyzed
11 correctly in 100% of cases against 75% of correct analyses from the lateral wall and 50%
12 from the anterior wall (Table 1). The mechanical wave front clearly propagated from the
13 endocardium towards the epicardium at a mean±SD speed of $1.1 \pm 0.35\text{ m}\cdot\text{s}^{-1}$.

14
15
16
17
18
19
20
21
22
23
24
25

1 **Discussion**

2 *EWI mapping allows accurate description of a focal ventricular activation*

3 Assessment of the activation through electromechanical wave front motion was effective:
4 endocardial versus epicardial stimulation were clearly distinguished using the location of the
5 initial activation and the direction of the wave front propagation. Sinus rhythm was
6 distinguished from paced rhythm using the shape of the wave front and the electromechanical
7 coupling. The present experiment was useful not only to visualize the origin of the
8 mechanical activation within the thickness of a cardiac wall, but also to provide data on the
9 behavior of the wave front into the muscle. Interferences that could jeopardize proper
10 interpretation were distinguished from the electromechanical activation by using the 3-times
11 recorded loops method. Although such a description is still in experimental phase, EWI
12 mapping is promising since the localization of intra myocardial *foci* may be critical during
13 catheter ablation procedures. It may provide real-time mechanistic insights by linking the
14 wave front speed to histological characteristics of the substrate and be complementary to
15 electro-anatomical mapping systems already available. This technique, more accurate, might
16 help in differentiating the origin of a VT (endocardial versus epicardial) and the underlying
17 mechanism (focal versus reentrance). So far, not a single reliable system enables such
18 observations.

19 *Technical concerns and observations*

20 In order to place pacemaker leads easily, at the endocardial and epicardial sides of the three
21 LV portions, experiments were conducted on an isolated working heart instead of a standard
22 in vivo setup. When placing the US probe against the heart, such installation avoids any
23 acoustic fences that can jeopardize the high-resolution activation recordings using an extra

1 cardiac probe. Since the recordings were performed under a time frame of 200ms and the
2 initiation of the EWI was visible during less than 50ms, global heart motion did not
3 jeopardize visualization. Even though the 15 MHz probe used prevented a large visual field
4 (only 14 mm x 14 mm square), it offered an accurate view of the muscle. Konofagou's group
5 recently demonstrated a correlation between EWI activation and global electrical activation in
6 a ventricle(Grondin et al. 2016)(Costet et al. 2016)(Provost et al. 2011). Their method
7 provides global activation mapping during sinus rhythm(Melki et al. 2017) or stimulated
8 rhythm(Bunting et al. 2017)(Costet et al. 2016). More recently, epicardial and endocardial
9 pacing were differentiated in 86% of cases(Costet et al. 2018) but results were based on only
10 eight measurements and did not take into account activation in sinus rhythm. The experiment
11 presented herein confirmed the possibility to differentiate between endocardial and epicardial
12 focal activation with similar rates and adds a complete analysis of the different segments of
13 the LV. Moreover, it allowed measuring of the wave front speed.
14 Finally, the loop-recorded images were confined to a small area but this technique will
15 eventually be able to provide data about a region of interest, once a 3-dimensionnal electro-
16 anatomical mapping is performed.

17

18 *Is there a correlation between myocardial structure and EWI?*

19

20 Different activation wave speeds were observed. The large difference between mechanical
21 and electrical waves reported to be around $0.5\text{m}\cdot\text{s}^{-1}$ in human hearts(Durrer et al. 1970) points
22 to the strong possibility that a mechanical wave - once initiated by the "kick" of an electrical
23 stimulus - mainly depends on the mechanical properties of the tissue. Wave front speed
24 changes could be related to the orientation of the myocardial fibers that follow different

1 directions before reaching the Purkinje system and may help to determine new properties of
2 the cardiac muscle.
3 Even though spatial resolution of the sequence presented herein prevents high-resolution
4 analysis of the activated wave front shape and speed, this technique might support the in vivo
5 correlation of anisotropic properties with the orientations of epicardial and endocardial
6 fibers(Deng et al. 2012), the anatomy of the Purkinje that usually contains more denser fibers
7 close to the endocardium(Garcia-Bustos et al. 2017), and the dispersion of the gap junction
8 density from the endocardium towards the epicardium(Yamada et al. 2004). Further
9 evaluations will be needed, combining information from a 3-dimensional histological analysis
10 of the interlaced fibers and a 3-dimensional ultrasound analysis of the area.

11

12 *Limitations*

13

14 The present study has some limitations. All images were obtained in swine hearts, in an
15 isolated bi-ventricular working mode with a 2-D probe. Results were therefore based on
16 mechanical recordings from a 2 dimensional space of an artificial endocardial and epicardial
17 paced activation. Moreover, since the hearts were healthy, no pathological substrate was
18 present inside the muscle. Even though 2-D spatial analyses sometimes prevented the wave
19 front to be clearly visible, the propagation of the electromechanical waves was looking
20 homogenous making the identification of the paced site easier and the calculation of the
21 mechanical wave front speed possible. Interestingly, global EWI mapping has already been
22 performed in sinus rhythm of myocardial infarction models(Costet et al. 2017), and on ablated
23 myocardium(Papadacci et al. 2017a). Since substrate analysis was successfully achieved in
24 those models, clinical application should be attainable. However, VT would induce more
25 complex schemes of activation in the three dimensions. Future experiments are needed using

1 a three-dimensional ultrasound and pathological models to determine the local EWI into a
2 scar and the ability of the system to determine a reentrant circuit.

3

4 *Ultrasound based mapping and its part in the future of electrophysiology*

5

6 Since the understanding of underlying mechanisms during VT ablation is one of the
7 cornerstones of a successful procedure, the type of acquisition presented here could be
8 integrated with electro-anatomical data, during catheter-based procedure, in order to improve
9 ablation success. This sequence could be embedded into an intra-cardiac echography (ICE)
10 system, avoiding any acoustic fences that could compromise quality of the images. Since ICE
11 already offers 2-D images and should be providing 3-D images in the next decade, the
12 addition of such sequences should allow a real-time “single beat” EWI activation map of
13 interlaced myocardial fibers inside an arrhythmic ventricle wall(Papadacci et al. 2017b).
14 Another option to limit acoustic fences would consist in providing such sequences under
15 transesophageal echocardiography (TEE) analysis, which already offers 2-D and 3-D
16 acquisitions. The combination of EWI mapping with elastography (available with ICE and
17 TEE) could provide both the location of the arrhythmia and the characteristics (shape, surface,
18 volume) of the thermal lesion after the ablation(Kwiecinski et al. 2015):(Kwiecinski et al.
19 2014):(Sandoval et al. 2018). Since high-intensity focused ultrasounds can be delivered from a
20 TEE(Bessiere et al. 2016):(Constanciel et al. 2013) into the ventricles, ultrasound energy
21 might be able, in the future, to localize, treat, and monitor cardiac arrhythmias.

22

23

24 **Conclusions**

25

1 EWI mapping allows assessment of mechanical activation of a LV wall in healthy hearts of an
2 isolated working mode system. Endocardial and epicardial pacing can be easily differentiated
3 from sinus rhythm activation and EWI-induced wave front can be accurately analyzed. This
4 technique is promising to provide help in differentiating between endocardial and epicardial
5 arrhythmias, during complex ablation procedures, and to characterize the mechanism of
6 ventricular activation. Future experiments will need to be conducted in diseased hearts, and
7 clinical data will be needed to correlate electrophysiological data to EWI activation patterns.

8

9

10

11

12

13

14

15

16 **Acknowledgements**

17 This work was supported by the French National Research Agency (ANR) under the
18 CHORUS Grant project ANR17-CE19-0017 and France Life Imaging – WP3 2019. Dr
19 Verena Landel is warmly thanked for her contribution and proofreading of the manuscript.

20

1 **References**

- 2
- 3 Bessiere F, N'djin WA, Colas EC, Chavrier F, Greillier P, Chapelon JY, Chevalier P, Lafon
4 C. Ultrasound-Guided Transesophageal High-Intensity Focused Ultrasound Cardiac Ablation
5 in a Beating Heart: A Pilot Feasibility Study in Pigs. *Ultrasound Med Biol* 2016;42:1848–
6 1861.
- 7 Bunting E, Lambrakos L, Kemper P, Whang W, Garan H, Konofagou E. Imaging the
8 Propagation of the Electromechanical Wave in Heart Failure Patients with Cardiac
9 Resynchronization Therapy. *Pacing Clin Electrophysiol PACE* 2017;40:35–45.
- 10 Constanciel E, N'Djin WA, Bessière F, Chavrier F, Grinberg D, Vignot A, Chevalier P,
11 Chapelon JY, Lafon C. Design and evaluation of a transesophageal HIFU probe for
12 ultrasound-guided cardiac ablation: simulation of a HIFU mini-maze procedure and
13 preliminary ex vivo trials. *IEEE Trans Ultrason Ferroelectr Freq Control* 2013;60:1868–1883.
- 14 Costet A, Melki L, Sayseng V, Hamid N, Nakanishi K, Wan E, Hahn R, Homma S,
15 Konofagou E. Electromechanical wave imaging and electromechanical wave velocity
16 estimation in a large animal model of myocardial infarction. *Phys Med Biol* 2017;62:9341–
17 9356.
- 18 Costet A, Wan E, Bunting E, Grondin J, Garan H, Konofagou E. Electromechanical wave
19 imaging (EWI) validation in all four cardiac chambers with 3D electroanatomic mapping in
20 canines in vivo. *Phys Med Biol* 2016;61:8105–8119.
- 21 Costet A, Wan E, Melki L, Bunting E, Grondin J, Garan H, Konofagou E. Non-invasive
22 Characterization of Focal Arrhythmia with Electromechanical Wave Imaging in Vivo.
23 *Ultrasound Med Biol* 2018;
- 24 Deng D, Jiao P, Ye X, Xia L. An image-based model of the whole human heart with detailed
25 anatomical structure and fiber orientation. *Comput Math Methods Med* 2012;2012:891070.

1 Durrer D, van Dam RT, Freud GE, Janse MJ, Meijler FL, Arzbacher RC. Total excitation of
2 the isolated human heart. *Circulation* 1970;41:899–912.

3 Enriquez A, Malavassi F, Saenz LC, Supple G, Santangeli P, Marchlinski FE, Garcia FC.
4 How to map and ablate left ventricular summit arrhythmias. *Heart Rhythm* 2017;14:141–148.

5 Erkapic D, Greiss H, Pajitnev D, Zaltsberg S, Deubner N, Berkowitsch A, Möllman S,
6 Sperzel J, Rolf A, Schmitt J, Hamm CW, Kuniss M, Neumann T. Clinical impact of a novel
7 three-dimensional electrocardiographic imaging for non-invasive mapping of ventricular
8 arrhythmias-a prospective randomized trial. *Eur Eur Pacing Arrhythm Card Electrophysiol J*
9 *Work Groups Card Pacing Arrhythm Card Cell Electrophysiol Eur Soc Cardiol* 2015;17:591–
10 597.

11 Fernandez-Armenta J, Berruezo A. How to recognize epicardial origin of ventricular
12 tachycardias? *Curr Cardiol Rev* 2014;10:246–256.

13 Garcia-Bustos V, Sebastian R, Izquierdo M, Molina P, Chorro FJ, Ruiz-Sauri A. A
14 quantitative structural and morphometric analysis of the Purkinje network and the Purkinje-
15 myocardial junctions in pig hearts. *J Anat* 2017;230:664–678.

16 Grondin J, Costet A, Bunting E, Gambhir A, Garan H, Wan E, Konofagou EE. Validation of
17 Electromechanical Wave Imaging in a canine model during pacing and sinus rhythm. *Heart*
18 *Rhythm Off J Heart Rhythm Soc* 2016;13:2221–2227.

19 J Shah A, Hocini M, Pascale P, Roten L, Komatsu Y, Daly M, Ramoul K, Denis A, Derval N,
20 Sacher F, Dubois R, Bokan R, Eliatou S, Strom M, Ramanathan C, Jais P, Ritter P,
21 Haissaguerre M. Body Surface Electrocardiographic Mapping for Non-invasive Identification
22 of Arrhythmic Sources. *Arrhythmia Electrophysiol Rev* 2013;2:16–22.

23 Kwiecinski W, Bessière F, Colas EC, N’Djin WA, Tanter M, Lafon C, Pernot M. Cardiac
24 shear-wave elastography using a transesophageal transducer: application to the mapping of
25 thermal lesions in ultrasound transesophageal cardiac ablation. *Phys Med Biol* 2015;60:7829–

1 7846.

2 Kwiecinski W, Provost J, Dubois R, Sacher F, Haïssaguerre M, Legros M, Nguyen-Dinh A,
3 Dufait R, Tanter M, Pernot M. Quantitative evaluation of atrial radio frequency ablation using
4 intracardiac shear-wave elastography. *Med Phys* 2014;41:112901.

5 Lerman BB. Mechanism, diagnosis, and treatment of outflow tract tachycardia. *Nat Rev*
6 *Cardiol* 2015;12:597–608.

7 Melki L, Costet A, Konofagou EE. Reproducibility and Angle Independence of
8 Electromechanical Wave Imaging for the Measurement of Electromechanical Activation
9 during Sinus Rhythm in Healthy Humans. *Ultrasound Med Biol* 2017;43:2256–2268.

10 Nguyen T-M, Song S, Arnal B, Huang Z, O’Donnell M, Wang RK. Visualizing ultrasonically
11 induced shear wave propagation using phase-sensitive optical coherence tomography for
12 dynamic elastography. *Opt Lett* 2014;39:838–841.

13 Papadacci C, Bunting EA, Wan EY, Nauleau P, Konofagou EE. 3D myocardial elastography
14 and electromechanical wave imaging in vivo. *IEEE Trans Med Imaging* 2017a;36:618–627.

15 Papadacci C, Finel V, Provost J, Villemain O, Bruneval P, Gennisson J-L, Tanter M, Fink M,
16 Pernot M. Imaging the dynamics of cardiac fiber orientation in vivo using 3D Ultrasound
17 Backscatter Tensor Imaging. *Sci Rep* 2017b;7:830.

18 Pinton GF, Dahl JJ, Trahey GE. Rapid tracking of small displacements with ultrasound. *IEEE*
19 *Trans Ultrason Ferroelectr Freq Control* 2006;53:1103–1117.

20 Provost J, Lee W-N, Fujikura K, Konofagou EE. Imaging the electromechanical activity of
21 the heart in vivo. *Proc Natl Acad Sci U S A* 2011;108:8565–8570.

22 Revishvili AS, Wissner E, Lebedev DS, Lemes C, Deiss S, Metzner A, Kalinin VV, Sopov
23 OV, Labartkava EZ, Kalinin AV, Chmelevsky M, Zubarev SV, Chaykovskaya MK, Tsiklauri
24 MG, Kuck K-H. Validation of the mapping accuracy of a novel non-invasive epicardial and
25 endocardial electrophysiology system. *Eur Eur Pacing Arrhythm Card Electrophysiol J Work*

1 Groups Card Pacing Arrhythm Card Cell Electrophysiol Eur Soc Cardiol 2015;17:1282–1288.
2 Sandoval Z, Castro M, Alirezaie J, Bessière F, Lafon C, Dillenseger J-L. Transesophageal 2D
3 ultrasound to 3D computed tomography registration for the guidance of a cardiac arrhythmia
4 therapy. *Phys Med Biol* 2018;63:155007.
5 Shivkumar K. Catheter Ablation of Ventricular Arrhythmias. *N Engl J Med* 2019;380:1555–
6 1564.
7 Vaillant F, Magat J, Bour P, Naulin J, Benoist D, Loyer V, Vieillot D, Labrousse L, Ritter P,
8 Bernus O, Dos Santos P, Quesson B. Magnetic resonance-compatible model of isolated
9 working heart from large animal for multimodal assessment of cardiac function,
10 electrophysiology, and metabolism. *Am J Physiol Heart Circ Physiol* 2016;310:H1371–1380.
11 Yamada KA, Kanter EM, Green KG, Saffitz JE. Transmural distribution of connexins in
12 rodent hearts. *J Cardiovasc Electrophysiol* 2004;15:710–715.
13
14
15
16
17
18
19
20
21
22
23
24

1 Table 1 Summary of the correct Electromechanical Wave Imaging (EWI) sequences
 2 interpretations from two independent readers

Activation origin			EPICARDIUM	ENDOCARDIUM	SINUS RHYTHM	TOTAL
SEGMENT	LATERAL	n	3/4	3/4	4/4	10/12
		%	75 %	75 %	100 %	83 %
	POSTERIOR	n	4/4	4/4	4/4	12/12
		%	100 %	100 %	100 %	100 %
	ANTERIOR	n	4/4	2/4	4/4	10/12
		%	100 %	50 %	100 %	83 %
	TOTAL	n	11/12	9/12	12/12	32/36
		%	92 %	75 %	100 %	89 %

3
 4
 5
 6
 7
 8
 9
 10
 11
 12
 13
 14
 15
 16
 17
 18

1 **Figure Captions**

2

3 Figure 1: Isolated working mode heart. The 15 MHz ultrasound (US) probe is facing the left
4 ventricle (LV). Two leads are screwed into the epicardial and endocardial sides of the LV.
5 The one on the endocardial side is placed through the left atrium, from a pulmonary vein.

6

7 Figure 2: The cross-cut view of the left ventricle depicts the relation between the epicardial
8 and endocardial leads and the ultrasound probe (short-axis).

9

10 Figure 3: Electromechanical wave imaging (EWI) in sinus rhythm. The first column shows
11 the electrocardiogram: from the first to the last line, a red dot depicts when the images were
12 recorded at four different moments of a cardiac cycle (ms). The second column shows the B-
13 mode corresponding images. The third column shows the corresponding EWI pictures
14 (deformation depicted in μm). The beginning of the induced electromechanical wave front is
15 wide, originating from the endocardium towards the epicardium.

16

17 Figure 4: EWI during epicardial pacing. The first column shows the electrocardiogram: from
18 the first to the last line, a red dot depicts when the images were recorded at four different
19 moments of a cardiac cycle (ms). The second column shows the B-mode corresponding
20 images. The third column shows the corresponding EWI pictures (deformation depicted in
21 μm). The beginning of the induced electromechanical wave front is focal and clearly
22 distinguished on the upper right corner of the image (in red). It corresponds to the location of
23 the epicardial lead.

24

1 Figure 5: EWI during endocardial pacing. The first column shows the electrocardiogram:
2 from the first to the last line, a red dot depicts when the images were recorded at four different
3 moments of a cardiac cycle (ms). The second column shows the B-mode corresponding
4 images. The third column shows the corresponding EWI pictures (deformation depicted in
5 μm). The beginning of the induced electromechanical wave front is focal and clearly
6 distinguished on the lower left corner of the image (in red). It corresponds to the location of
7 the endocardial lead.

8

1 **High frame rate ultrasound for electromechanical wave**
2 **imaging to differentiate endocardial from epicardial**
3 **myocardial activation**

4
5 Francis Bessière MD MSc^{1,2,3}, Ali Zorgani PhD^{2,3}, Jade Robert MSc^{2,3}, Loïc Daunizeau
6 MSc^{2,3}, Elodie Cao MSc^{2,3}, Fanny Vaillant PhD^{4,5,6}, Emma Abell MSc^{4,5,6}, Bruno Quesson
7 PhD^{4,5,6}, Stéphane Catheline PhD^{2,3}, Philippe Chevalier MD PhD^{1,3}, Cyril Lafon PhD^{2,3}

8
9 *1- Hôpital cardiologique Louis Pradel, Hospices Civils de Lyon, 69677 Lyon, France*

10 *2- LabTAU, INSERM, Centre Léon Bérard, Université Lyon 1, Univ Lyon, F-69003,*
11 *LYON, France*

12 *3- Université de Lyon, France*

13 *4- IHU Liryc, Electrophysiology and Heart Modeling Institute, fondation Bordeaux*
14 *Université, 33600 Pessac-Bordeaux, France*

15 *5- Université de Bordeaux, Centre de recherche Cardio-Thoracique de Bordeaux,*
16 *U1045, 33000, Bordeaux, France*

17 *6- INSERM, Centre de recherche Cardio-Thoracique de Bordeaux, U1045, 33000*
18 *Bordeaux, France*

19

20

21 None of the authors report any conflict of interest

22

1 Corresponding author:

2 Dr Francis BESSIERE

3 Electrophysiology department, Louis Pradel Cardiovascular Hospital

4 59 boulevard Pinel, 69500 Bron, France

5 E mail : francis.bessiere@chu-lyon.fr

6 Tel : +33472119075

7

8

9

10

11

12

13

14

15

16

17

18

19

20

21

22

23

24

1 **Abstract**

2

3 Differentiation between epicardial and endocardial ventricular activation remains a challenge,
4 despite the latest technologies available. The aim of the present study was to develop a new
5 tool method, based on electromechanical wave imaging (EWI), to improve arrhythmogenic
6 substrate activation analysis. Experiments were conducted on left ventricles (LV) of four
7 isolated working mode swine hearts. The protocol aimed at demonstrating that different
8 patterns of mechanical activation could be observed whether the ventricle was in sinus
9 rhythm, paced from the epicardium, or from the endocardium. Seventy-two EWI acquisitions
10 were recorded on the anterior, lateral, and posterior segments of the LV. Fifty-four loop
11 records were blindly assigned to two readers. EWI sequences interpretations were correct in
12 89% of cases. The overall agreement rate between the two readers was 83%. When in a
13 paced ventricle, the origin of the wave front was focal and originated from the endocardium
14 or the epicardium. In sinus rhythm, wave front was global and activated within the entire
15 endocardium towards the epicardium at a speed of 1.7 ± 0.28 m.s⁻¹. Wave front speeds were
16 respectively measured when the endocardium or the epicardium were paced at a speed of 1.1
17 ± 0.35 m.s⁻¹ vs 1.3 ± 0.34 m.s⁻¹ (p=NS). EWI activation mapping allows activation
18 localization within the LV wall and calculation of the wave front propagation speed through
19 the muscle. In the future, this technology could help localize activation within the LV
20 thickness during complex ablation procedures.

21

22

23 **Keywords:** Electromechanical wave imaging; ventricular arrhythmia; endocardial versus
24 epicardial activation; cardiac mapping; ultrasound

25

1 **Introduction**

2

3 Many options are available to delineate the electrophysiological and anatomical substrates of
4 ventricular arrhythmia, whether it concerns premature ventricular contraction (PVC) or
5 ventricular tachycardia (VT). The electrocardiogram (ECG) is the oldest option. QRS
6 complex duration, polarity, and morphology analysis from a 12-lead surface trace provides
7 clues on the location of the arrhythmia inside the ventricles. However, ECG lacks precision
8 since it is difficult to localize the origin of a *foci* within the thickness of the wall. Such
9 difficulties have already been reported when differentiating endocardial from epicardial
10 VT(Fernandez-Armenta and Berruezo 2014) in the left ventricle (LV), and when attempting
11 to localize PVC in the outflow tract (Lerman 2015)(Enriquez et al. 2017). Recently, high-
12 density extra-cardiac mapping has been developed. A 252-lead surface acquisition merged
13 onto a three dimensional cardiac tomography reconstruction provides real time activation
14 mapping to localize the arrhythmia source (J Shah et al. 2013)(Revishvili et al. 2015)(Erkagic
15 et al. 2015). This promising technology can be used to locate occult paroxysmal arrhythmia
16 during catheter ablation procedures. However, this method is expensive and lacks precision
17 since the body surface acquisition is only able to show the first area activated. In the case of
18 PVC or VT, the system cannot distinguish endocardial from epicardial origin, as the electrical
19 recordings at the surface of the thorax combine information from the entire thickness of the
20 ventricles. A bipolar catheter-based endocardial and epicardial activation mapping system can
21 also be used to more precisely localize the arrhythmia. In such a context, if the underlying
22 electrophysiological mechanism is hyper automatism, it usually allows the localization of a
23 PVC or a VT and when it is a reentrant circuit, the critical isthmus may be determined
24 effectively. However, this technique requires time to yield reliable and useful information to
25 locate and treat the arrhythmia substrate. Sometimes, the exact location of a PVC or VT

1 remains unclear, since it may come from the mid myocardium, or an area that cannot be
2 reached easily by an intra-cardiac catheter (i.e: LV summit)(Enriquez et al. 2017). Moreover,
3 this method remains risky since epicardial access may lead to coronary artery injuries, cardiac
4 perforation, or chronic pericarditis and endocardial access may cause strokes(Shivkumar
5 2019).

6 Ultrasonic quantitative mapping of myocardial activation has been shown to provide global
7 activation maps. High rate recordings from myocardial deformation are gated by the
8 electrocardiogram in such a way that motion can be decomposed while the ECG runs to create
9 the electromechanical wave imaging (EWI). This has been shown to be effective in mapping
10 sinus rhythm activation(Melki et al. 2017) or stimulated rhythm(Bunting et al. 2017)(Costet
11 et al. 2016) in animal models with healthy, infarcted(Costet et al. 2017), or ablated
12 hearts(Papadacci et al. 2017a). More recently, EWI was able to differentiate endocardial from
13 epicardial foci (Costet et al. 2018). However, only eight measurements were performed and
14 interpretation was done in a non-blinded manner, preventing a statistically relevant conclusion
15 to be given. In the present preliminary study, experiments were conducted in swine healthy
16 hearts of an isolated working heart model(Vaillant et al. 2016) using local bipolar electrogram
17 signal gated EWI. The aim was to describe local high-resolution endocardial and epicardial
18 activation patterns and characterize wave front propagation within the thickness of the LV
19 wall. Reliability of this method was provided from EWI records of the anterior, lateral, and
20 posterior walls of the LV.

21

22

1 **Materials and Methods**

2 *Animal preparation*

3 The study protocol was approved by the local Animal Research Ethics Committee (CEEA50)
4 in accordance with recommendations of the Directive 2010/63/EU of the European
5 Parliament on the protection of animals used for scientific purposes. Pigs (Large White
6 Landrace, 40 kg, $n = 4$) were pre-medicated with an intramuscular injection of ketamine (20
7 mg/kg), acepromazine (0.1 mg/kg), and buprenorphine (10 $\mu\text{g}/\text{kg}$). Anesthesia was induced
8 with an intravenous bolus of propofol (1 mg/kg) and maintained with ketamine and
9 midazolam (40 $\text{mg}\cdot\text{kg}^{-1}\cdot\text{h}^{-1}$ and 2 $\text{mg}\cdot\text{kg}^{-1}\cdot\text{h}^{-1}$, respectively). Animals were then intubated and
10 ventilated (50/50 air/oxygen), and received an injection of heparin (200 UI/kg).

11 *Excision and perfusion*

12 The swine thorax was opened, and blood was collected (2 L) via the introduction of an 8-Fr
13 sheath into the right jugular vein. Heparin (2500 UI/L) was added in the reservoir to avoid
14 coagulation. Heart was excised according to protocols used in humans during heart
15 transplantation; cardiac arrest was performed in vivo by cross clamping of the ascending aorta
16 and direct injection into the aortic root of 1L of cold (4°C) cardioplegic homemade Custodiol
17 (in mM: NaCl 15, KCl 9, MgCl₂ 4, α -ketoglutaric acid 1, histidine.HCl.H₂O 18, histidine
18 180, tryptophan 2, mannitol 30, CaCl₂ 0.015), before rapid excision and immersion in a cold
19 0.9% saline solution. The aorta, pulmonary artery, pulmonary veins, and superior vena cava
20 were cannulated to perfuse the heart in the isolated working mode. Inferior vena cava vein
21 was sutured to limit leaks.

22 *Isolated heart perfusion in recirculating biventricular-working mode*

1 The chambers used for preload, afterload, and aortic compliance were made from a 1 liter
2 water- jacketed glassware (Radnoti LLC, Monrovia, California, USA) to control the perfusate
3 temperature. Heart reperfusion was performed in the Langendorff mode for 15–20 min to
4 wash out the cardioplegic solution, gradually rewarm the heart and recover a stable ex vivo
5 cardiac function. The Langendorff perfusion pressure was adjusted to achieve 60 mmHg. If
6 necessary, the heart was defibrillated at 10–30 J (Life Pak 12, Medtronic, Minneapolis,
7 Minnesota, USA). The heart was perfused with blood collected on the same animal before
8 heart excision, diluted with a Tyrode buffer (vol/vol: 1/5; in mM: NaCl 128, KCl 4.7, MgCl₂
9 0.7, NaH₂PO₄ 0.5, NaHCO₃ 28, CaCl₂ 1.8, Glucose 11, Pyruvate 0.5, Lactate 1, Mannitol 16).
10 The perfusion medium was gassed with a mix of 95%/5% oxygen for maximal oxygenation
11 and maintained at pH 7.4 and at 37.5°C. A clinical oxygenator and arterial filter (Getinge
12 Group, Rastatt, Bade-Wurtemberg, Germany) were added before the preload reservoir to
13 ensure an optimal oxygenation of the perfusion medium. After stabilization (10 min with
14 spontaneous cardiac rhythm), the system was switched from Langendorff to working mode.
15 Pre- and afterloads were maintained constant during the whole protocol (left atrial pressure:
16 10–15 mmHg; right atrial pressure: 5-10 mmHg; left ventricular afterload: 70-90 mmHg; right
17 ventricular afterload: 15-30 mmHg).

18

19 *Lead placement and pacing protocol*

20

21 Six pacemaker leads (Tendril 52cm, Abbott, Minneapolis, Minnesota, USA) were fixed in
22 pairs, on the anterior, lateral, and posterior walls of the LV. The epicardial leads were
23 attached on the epicardium of the designated portion; under ultrasound guidance endocardial
24 leads were screwed at the exact opposite side of the wall, in such a way that the exact same
25 portion of the LV could be paced from the endocardium or the epicardium. A schematic view

1 and description of the setup is shown in Figures 1 & 2. Each lead was successively connected
2 via a wire to a device controller (Merlin, Abbott, Minneapolis, Minnesota, USA). Pacing
3 parameters were settled 0.2 V above the threshold to get a local capture that would not
4 jeopardize activation mapping within the LV wall. The duration of the stimulus was set at 0.4
5 ms. Sites were consecutively paced 20 bpm above the spontaneous sinus rhythm.

6

7 *Ultrasound acquisition*

8

9 A 15 MHz central frequency ultrasonic probe (L15-Xtech, Vermon, Tours, France) was
10 placed facing the LV wall (Figure 2) and maintained by a hydraulic flexible arm in the same
11 position during the whole experiment. The 2-dimensional probe was connected to an ultrafast
12 ultrasound scanner (Vantage, Verasonics, Kirkland, Washington, USA). Conventional B-
13 mode images were acquired in the short-axis at 50 frames/second to assist myocardial
14 segmentation and to guide the placement of the pacing electrodes. After placing two
15 electrodes at the surface of the heart, a bipolar signal was acquired using an ECG unit (DAM
16 50, Word Precision Instrument, Sarasota, Florida, USA) and recorded using an oscilloscope
17 (PicoScope 3000, Pico Technology, St Neots, UK).

18 An ultrafast imaging sequence was used to acquire 400 B-mode images at a pulse repetition
19 frequency of 2500 frames/second on the first heart (160ms). The last three hearts were
20 recorded using 800 B-mode images acquisition at a pulse repetition frequency of 4000
21 frames/second (200ms), during sinus rhythm, pericardial, or endocardial pacing to maximize
22 the accuracy of the measurements. In order to synchronize the ultrafast acquisition with the
23 bipolar signal wave, an output signal was generated for each frame and superimposed on the
24 bipolar signal. A phase-based motion tracking estimation algorithm(Pinton et al. 2006) was
25 applied to the radiofrequency (RF) data in order to track the electromechanical wave

1 propagation into the LV wall. Unlike speckle tracking algorithm based on RF-Window cross-
2 correlation, this method allows conservation of high spatial resolution of the initial B-mode
3 images.

4

5 *EWI interpretation*

6

7 A total of 4 isolated hearts were analyzed successively. The experiments on the first 2 hearts
8 were carried out to validate the proof of concept. Loops from the anterior wall on the left
9 ventricle were analyzed to describe the scheme of activation when the electrical activation
10 was coming from the epicardium, the endocardium, and in sinus rhythm. Based on the
11 observations from the first 2 hearts, the last 2 hearts were carried out to evaluate the ability of
12 the system to detect the different patterns of mechanical activation when blinded to the
13 electrical activation. Three segments of the LV were successively analyzed: the anterior wall,
14 the lateral wall, and the posterior wall. For every segment and activation mode, EWI loops
15 were recorded three times. Two separate readers (JR and EC) received training based of the
16 observations obtained from the first 2 hearts. Then, blinded to the electrical activation, the
17 same authors qualitatively interpreted the 3-recorded loops of a segment to be in accordance
18 with the predetermined sinus rhythm, endocardial pacing, and epicardial pacing patterns. A
19 sequence of a 3-times recorded loop was considered in accordance when at least 2 of the 3
20 loops were consistent with predetermined patterns. The axial propagation speeds of the wave
21 fronts were computed based on a time of flight method along the thickness of the myocardium
22 wall (i.e. time vs space representation)(Nguyen et al. 2014). Quantitative (mean \pm standard
23 deviation (SD)) and qualitative (%) variables were analyzed. Overall agreement analyses were
24 performed using the Cohen's Kappa index.

25

1 **Results**

2

3 From the first two hearts, 6 EWI sequences were collected and analyzed: 2 in sinus rhythm, 2
4 in epicardial pacing, and 2 in endocardial pacing. EWI sequences were each made by a 3-
5 recordings of the zone (= 18 loops). In sinus rhythm, visual qualitative displays of the wave
6 front scheme were similar between all recordings: the EWI-induced wave front systematically
7 originated from the endocardium and mid myocardium and moved towards the epicardium
8 with a wide and global displacement (Figure 3). During epicardial and endocardial pacing,
9 visual qualitative displays of the wave front demonstrated a focal positive displacement after
10 rising of the local electrical signal. When visible, the origin of the EWI activation matched the
11 location of the epicardial or endocardial leads (Figures 4 and 5).

12

13 From the last two hearts, 18 EWI sequences were collected: 6 in sinus rhythm, 6 in epicardial
14 pacing, and 6 in endocardial pacing. EWI sequences were each made by a 3-recordings of the
15 zone (= 54 loops). Every sequence in sinus rhythm, epicardial pacing, and endocardial pacing
16 were all collected 2 times on the anterior, lateral wall, and posterior walls. Two independent
17 readers analyzed all sequences to provide descriptive statistics (36 lectures = 108 loops
18 analyzed).

19

20 In spontaneous sinus rhythm, the mean \pm SD heart rate was 119 \pm 6bpm; the epicardium and
21 endocardium sides were sequentially paced at a mean \pm SD rate of 138 \pm 9bpm.

22 EWI sequences readings matched the electrical activation in 89% of cases (Table 1). The
23 overall agreement rate between the two readers was 83%.

1 The readers differentiated in 100% of cases, paced from sinus rhythm activations, on the
2 anterior, the lateral, and the posterior walls. Mean±SD propagation speed of the mechanical
3 wave front in sinus rhythm, into the thickness of the muscle, was 1.7 ± 0.28 m.s⁻¹.
4 EWI acquisitions allowed epicardial activation detection in 92% of cases. When on the
5 posterior or anterior walls, activation patterns from the epicardium were analyzed correctly in
6 100% of cases. When on the lateral wall, only 75% of correct analysis was observed (Table
7 1). The mechanical wave front started in a focal zone where the lead was located, and
8 propagated from the epicardium towards the endocardium at a mean±SD speed of 1.3 ± 0.34
9 m.s⁻¹. EWI acquisitions allowed endocardial activation detection in 75% of cases. When on
10 the posterior wall, activation patterns detected from the endocardial lead were analyzed
11 correctly in 100% of cases against 75% of correct analyses from the lateral wall and 50%
12 from the anterior wall (Table 1). The mechanical wave front clearly propagated from the
13 endocardium towards the epicardium at a mean±SD speed of 1.1 ± 0.35 m.s⁻¹.

14
15
16
17
18
19
20
21
22
23
24
25

1 **Discussion**

2 *EWI mapping allows accurate description of a focal ventricular activation*

3 Assessment of the activation through electromechanical wave front motion was effective:
4 endocardial versus epicardial stimulation were clearly distinguished using the location of the
5 initial activation and the direction of the wave front propagation. Sinus rhythm was
6 distinguished from paced rhythm using the shape of the wave front and the electromechanical
7 coupling. The present experiment was useful not only to visualize the origin of the
8 mechanical activation within the thickness of a cardiac wall, but also to provide data on the
9 behavior of the wave front into the muscle. Interferences that could jeopardize proper
10 interpretation were distinguished from the electromechanical activation by using the 3-times
11 recorded loops method. Although such a description is still in experimental phase, EWI
12 mapping is promising since the localization of intra myocardial *foci* may be critical during
13 catheter ablation procedures. It may provide real-time mechanistic insights by linking the
14 wave front speed to histological characteristics of the substrate and be complementary to
15 electro-anatomical mapping systems already available. This technique, more accurate, might
16 help in differentiating the origin of a VT (endocardial versus epicardial) and the underlying
17 mechanism (focal versus reentrance). So far, not a single reliable system enables such
18 observations.

19 *Technical concerns and observations*

20 In order to place pacemaker leads easily, at the endocardial and epicardial sides of the three
21 LV portions, experiments were conducted on an isolated working heart instead of a standard
22 in vivo setup. When placing the US probe against the heart, such installation avoids any
23 acoustic fences that can jeopardize the high-resolution activation recordings using an extra

1 cardiac probe. Since the recordings were performed under a time frame of 200ms and the
2 initiation of the EWI was visible during less than 50ms, global heart motion did not
3 jeopardize visualization. Even though the 15 MHz probe used prevented a large visual field
4 (only 14 mm x 14 mm square), it offered an accurate view of the muscle. Konofagou's group
5 recently demonstrated a correlation between EWI activation and global electrical activation in
6 a ventricle(Grondin et al. 2016)(Costet et al. 2016)(Provost et al. 2011). Their method
7 provides global activation mapping during sinus rhythm(Melki et al. 2017) or stimulated
8 rhythm(Bunting et al. 2017)(Costet et al. 2016). More recently, epicardial and endocardial
9 pacing were differentiated in 86% of cases(Costet et al. 2018) but results were based on only
10 eight measurements and did not take into account activation in sinus rhythm. The experiment
11 presented herein confirmed the possibility to differentiate between endocardial and epicardial
12 focal activation with similar rates and adds a complete analysis of the different segments of
13 the LV. Moreover, it allowed measuring of the wave front speed.
14 Finally, the loop-recorded images were confined to a small area but this technique will
15 eventually be able to provide data about a region of interest, once a 3-dimensionnal electro-
16 anatomical mapping is performed.

17

18 *Is there a correlation between myocardial structure and EWI?*

19

20 Different activation wave speeds were observed. The large difference between mechanical
21 and electrical waves reported to be around $0.5\text{m}\cdot\text{s}^{-1}$ in human hearts(Durrer et al. 1970) points
22 to the strong possibility that a mechanical wave - once initiated by the "kick" of an electrical
23 stimulus - mainly depends on the mechanical properties of the tissue. Wave front speed
24 changes could be related to the orientation of the myocardial fibers that follow different

1 directions before reaching the Purkinje system and may help to determine new properties of
2 the cardiac muscle.

3 Even though spatial resolution of the sequence presented herein prevents high-resolution
4 analysis of the activated wave front shape and speed, this technique might support the in vivo
5 correlation of anisotropic properties with the orientations of epicardial and endocardial
6 fibers(Deng et al. 2012), the anatomy of the Purkinje that usually contains more denser fibers
7 close to the endocardium(Garcia-Bustos et al. 2017), and the dispersion of the gap junction
8 density from the endocardium towards the epicardium(Yamada et al. 2004). Further
9 evaluations will be needed, combining information from a 3-dimensional histological analysis
10 of the interlaced fibers and a 3-dimensional ultrasound analysis of the area.

11

12 *Limitations*

13

14 The present study has some limitations. All images were obtained in swine hearts, in an
15 isolated bi-ventricular working mode with a 2-D probe. Results were therefore based on
16 mechanical recordings from a 2 dimensional space of an artificial endocardial and epicardial
17 paced activation. Moreover, since the hearts were healthy, no pathological substrate was
18 present inside the muscle. Even though 2-D spatial analyses sometimes prevented the wave
19 front to be clearly visible, the propagation of the electromechanical waves was looking
20 homogenous making the identification of the paced site easier and the calculation of the
21 mechanical wave front speed possible. Interestingly, global EWI mapping has already been
22 performed in sinus rhythm of myocardial infarction models(Costet et al. 2017), and on ablated
23 myocardium(Papadacci et al. 2017a). Since substrate analysis was successfully achieved in
24 those models, clinical application should be attainable. However, VT would induce more
25 complex schemes of activation in the three dimensions. Future experiments are needed using

1 a three-dimensional ultrasound and pathological models to determine the local EWI into a
2 scar and the ability of the system to determine a reentrant circuit.

3

4 *Ultrasound based mapping and its part in the future of electrophysiology*

5

6 Since the understanding of underlying mechanisms during VT ablation is one of the
7 cornerstones of a successful procedure, the type of acquisition presented here could be
8 integrated with electro-anatomical data, during catheter-based procedure, in order to improve
9 ablation success. This sequence could be embedded into an intra-cardiac echography (ICE)
10 system, avoiding any acoustic fences that could compromise quality of the images. Since ICE
11 already offers 2-D images and should be providing 3-D images in the next decade, the
12 addition of such sequences should allow a real-time “single beat” EWI activation map of
13 interlaced myocardial fibers inside an arrhythmic ventricle wall(Papadacci et al. 2017b).
14 Another option to limit acoustic fences would consist in providing such sequences under
15 transesophageal echocardiography (TEE) analysis, which already offers 2-D and 3-D
16 acquisitions. The combination of EWI mapping with elastography (available with ICE and
17 TEE) could provide both the location of the arrhythmia and the characteristics (shape, surface,
18 volume) of the thermal lesion after the ablation(Kwiecinski et al. 2015):(Kwiecinski et al.
19 2014):(Sandoval et al. 2018). Since high-intensity focused ultrasounds can be delivered from a
20 TEE(Bessiere et al. 2016):(Constanciel et al. 2013) into the ventricles, ultrasound energy
21 might be able, in the future, to localize, treat, and monitor cardiac arrhythmias.

22

23

24

25

1 **Conclusions**

2

3 EWI mapping allows assessment of mechanical activation of a LV wall in healthy hearts of an
4 isolated working mode system. Endocardial and epicardial pacing can be easily differentiated
5 from sinus rhythm activation and EWI-induced wave front can be accurately analyzed. This
6 technique is promising to provide help in differentiating between endocardial and epicardial
7 arrhythmias, during complex ablation procedures, and to characterize the mechanism of
8 ventricular activation. Future experiments will need to be conducted in diseased hearts, and
9 clinical data will be needed to correlate electrophysiological data to EWI activation patterns.

10

11

12

13

14

15

16

17

18 **Acknowledgements**

19 This work was supported by the French National Research Agency (ANR) under the
20 CHORUS Grant project ANR17-CE19-0017 and France Life Imaging – WP3 2019. Dr
21 Verena Landel is warmly thanked for her contribution and proofreading of the manuscript.

22

1 **References**

- 2
- 3 Bessiere F, N'djin WA, Colas EC, Chavrier F, Greillier P, Chapelon JY, Chevalier P, Lafon
4 C. Ultrasound-Guided Transesophageal High-Intensity Focused Ultrasound Cardiac Ablation
5 in a Beating Heart: A Pilot Feasibility Study in Pigs. *Ultrasound Med Biol* 2016;42:1848–
6 1861.
- 7 Bunting E, Lambrakos L, Kemper P, Whang W, Garan H, Konofagou E. Imaging the
8 Propagation of the Electromechanical Wave in Heart Failure Patients with Cardiac
9 Resynchronization Therapy. *Pacing Clin Electrophysiol PACE* 2017;40:35–45.
- 10 Constanciel E, N'Djin WA, Bessière F, Chavrier F, Grinberg D, Vignot A, Chevalier P,
11 Chapelon JY, Lafon C. Design and evaluation of a transesophageal HIFU probe for
12 ultrasound-guided cardiac ablation: simulation of a HIFU mini-maze procedure and
13 preliminary ex vivo trials. *IEEE Trans Ultrason Ferroelectr Freq Control* 2013;60:1868–1883.
- 14 Costet A, Melki L, Sayseng V, Hamid N, Nakanishi K, Wan E, Hahn R, Homma S,
15 Konofagou E. Electromechanical wave imaging and electromechanical wave velocity
16 estimation in a large animal model of myocardial infarction. *Phys Med Biol* 2017;62:9341–
17 9356.
- 18 Costet A, Wan E, Bunting E, Grondin J, Garan H, Konofagou E. Electromechanical wave
19 imaging (EWI) validation in all four cardiac chambers with 3D electroanatomic mapping in
20 canines in vivo. *Phys Med Biol* 2016;61:8105–8119.
- 21 Costet A, Wan E, Melki L, Bunting E, Grondin J, Garan H, Konofagou E. Non-invasive
22 Characterization of Focal Arrhythmia with Electromechanical Wave Imaging in Vivo.
23 *Ultrasound Med Biol* 2018;
- 24 Deng D, Jiao P, Ye X, Xia L. An image-based model of the whole human heart with detailed
25 anatomical structure and fiber orientation. *Comput Math Methods Med* 2012;2012:891070.

1 Durrer D, van Dam RT, Freud GE, Janse MJ, Meijler FL, Arzbacher RC. Total excitation of
2 the isolated human heart. *Circulation* 1970;41:899–912.

3 Enriquez A, Malavassi F, Saenz LC, Supple G, Santangeli P, Marchlinski FE, Garcia FC.
4 How to map and ablate left ventricular summit arrhythmias. *Heart Rhythm* 2017;14:141–148.

5 Erkapic D, Greiss H, Pajitnev D, Zaltsberg S, Deubner N, Berkowitsch A, Möllman S,
6 Sperzel J, Rolf A, Schmitt J, Hamm CW, Kuniss M, Neumann T. Clinical impact of a novel
7 three-dimensional electrocardiographic imaging for non-invasive mapping of ventricular
8 arrhythmias-a prospective randomized trial. *Eur Eur Pacing Arrhythm Card Electrophysiol J*
9 *Work Groups Card Pacing Arrhythm Card Cell Electrophysiol Eur Soc Cardiol* 2015;17:591–
10 597.

11 Fernandez-Armenta J, Berruezo A. How to recognize epicardial origin of ventricular
12 tachycardias? *Curr Cardiol Rev* 2014;10:246–256.

13 Garcia-Bustos V, Sebastian R, Izquierdo M, Molina P, Chorro FJ, Ruiz-Sauri A. A
14 quantitative structural and morphometric analysis of the Purkinje network and the Purkinje-
15 myocardial junctions in pig hearts. *J Anat* 2017;230:664–678.

16 Grondin J, Costet A, Bunting E, Gambhir A, Garan H, Wan E, Konofagou EE. Validation of
17 Electromechanical Wave Imaging in a canine model during pacing and sinus rhythm. *Heart*
18 *Rhythm Off J Heart Rhythm Soc* 2016;13:2221–2227.

19 J Shah A, Hocini M, Pascale P, Roten L, Komatsu Y, Daly M, Ramoul K, Denis A, Derval N,
20 Sacher F, Dubois R, Bokan R, Eliatou S, Strom M, Ramanathan C, Jais P, Ritter P,
21 Haissaguerre M. Body Surface Electrocardiographic Mapping for Non-invasive Identification
22 of Arrhythmic Sources. *Arrhythmia Electrophysiol Rev* 2013;2:16–22.

23 Kwiecinski W, Bessière F, Colas EC, N’Djin WA, Tanter M, Lafon C, Pernot M. Cardiac
24 shear-wave elastography using a transesophageal transducer: application to the mapping of
25 thermal lesions in ultrasound transesophageal cardiac ablation. *Phys Med Biol* 2015;60:7829–

1 7846.

2 Kwiecinski W, Provost J, Dubois R, Sacher F, Haïssaguerre M, Legros M, Nguyen-Dinh A,
3 Dufait R, Tanter M, Pernot M. Quantitative evaluation of atrial radio frequency ablation using
4 intracardiac shear-wave elastography. *Med Phys* 2014;41:112901.

5 Lerman BB. Mechanism, diagnosis, and treatment of outflow tract tachycardia. *Nat Rev*
6 *Cardiol* 2015;12:597–608.

7 Melki L, Costet A, Konofagou EE. Reproducibility and Angle Independence of
8 Electromechanical Wave Imaging for the Measurement of Electromechanical Activation
9 during Sinus Rhythm in Healthy Humans. *Ultrasound Med Biol* 2017;43:2256–2268.

10 Nguyen T-M, Song S, Arnal B, Huang Z, O’Donnell M, Wang RK. Visualizing ultrasonically
11 induced shear wave propagation using phase-sensitive optical coherence tomography for
12 dynamic elastography. *Opt Lett* 2014;39:838–841.

13 Papadacci C, Bunting EA, Wan EY, Nauleau P, Konofagou EE. 3D myocardial elastography
14 and electromechanical wave imaging in vivo. *IEEE Trans Med Imaging* 2017a;36:618–627.

15 Papadacci C, Finel V, Provost J, Villemain O, Bruneval P, Gennisson J-L, Tanter M, Fink M,
16 Pernot M. Imaging the dynamics of cardiac fiber orientation in vivo using 3D Ultrasound
17 Backscatter Tensor Imaging. *Sci Rep* 2017b;7:830.

18 Pinton GF, Dahl JJ, Trahey GE. Rapid tracking of small displacements with ultrasound. *IEEE*
19 *Trans Ultrason Ferroelectr Freq Control* 2006;53:1103–1117.

20 Provost J, Lee W-N, Fujikura K, Konofagou EE. Imaging the electromechanical activity of
21 the heart in vivo. *Proc Natl Acad Sci U S A* 2011;108:8565–8570.

22 Revishvili AS, Wissner E, Lebedev DS, Lemes C, Deiss S, Metzner A, Kalinin VV, Sopov
23 OV, Labartkava EZ, Kalinin AV, Chmelevsky M, Zubarev SV, Chaykovskaya MK, Tsiklauri
24 MG, Kuck K-H. Validation of the mapping accuracy of a novel non-invasive epicardial and
25 endocardial electrophysiology system. *Eur Eur Pacing Arrhythm Card Electrophysiol J Work*

1 Groups Card Pacing Arrhythm Card Cell Electrophysiol Eur Soc Cardiol 2015;17:1282–1288.
2 Sandoval Z, Castro M, Alirezaie J, Bessière F, Lafon C, Dillenseger J-L. Transesophageal 2D
3 ultrasound to 3D computed tomography registration for the guidance of a cardiac arrhythmia
4 therapy. *Phys Med Biol* 2018;63:155007.
5 Shivkumar K. Catheter Ablation of Ventricular Arrhythmias. *N Engl J Med* 2019;380:1555–
6 1564.
7 Vaillant F, Magat J, Bour P, Naulin J, Benoist D, Loyer V, Vieillot D, Labrousse L, Ritter P,
8 Bernus O, Dos Santos P, Quesson B. Magnetic resonance-compatible model of isolated
9 working heart from large animal for multimodal assessment of cardiac function,
10 electrophysiology, and metabolism. *Am J Physiol Heart Circ Physiol* 2016;310:H1371–1380.
11 Yamada KA, Kanter EM, Green KG, Saffitz JE. Transmural distribution of connexins in
12 rodent hearts. *J Cardiovasc Electrophysiol* 2004;15:710–715.
13
14
15
16
17
18
19
20
21
22
23
24

1 Table 1 Summary of the correct Electromechanical Wave Imaging (EWI) sequences
 2 interpretations from two independent readers

Activation origin			EPICARDIUM	ENDOCARDIUM	SINUS RHYTHM	TOTAL
SEGMENT	LATERAL	n	3/4	3/4	4/4	10/12
		%	75 %	75 %	100 %	83 %
	POSTERIOR	n	4/4	4/4	4/4	12/12
		%	100 %	100 %	100 %	100 %
	ANTERIOR	n	4/4	2/4	4/4	10/12
		%	100 %	50 %	100 %	83 %
	TOTAL	n	11/12	9/12	12/12	32/36
		%	92 %	75 %	100 %	89 %

3
 4
 5
 6
 7
 8
 9
 10
 11
 12
 13
 14
 15
 16
 17
 18

1 **Figure Captions**

2

3 Figure 1: Isolated working mode heart. The 15 MHz ultrasound (US) probe is facing the left
4 ventricle (LV). Two leads are screwed into the epicardial and endocardial sides of the LV.
5 The one on the endocardial side is placed through the left atrium, from a pulmonary vein.

6

7 Figure 2: The cross-cut view of the left ventricle depicts the relation between the epicardial
8 and endocardial leads and the ultrasound probe (short-axis).

9

10 Figure 3: Electromechanical wave imaging (EWI) in sinus rhythm. The first column shows
11 the electrocardiogram: from the first to the last line, a red dot depicts when the images were
12 recorded at four different moments of a cardiac cycle (ms). The second column shows the B-
13 mode corresponding images. The third column shows the corresponding EWI pictures
14 (deformation depicted in μm). The beginning of the induced electromechanical wave front is
15 wide, originating from the endocardium towards the epicardium.

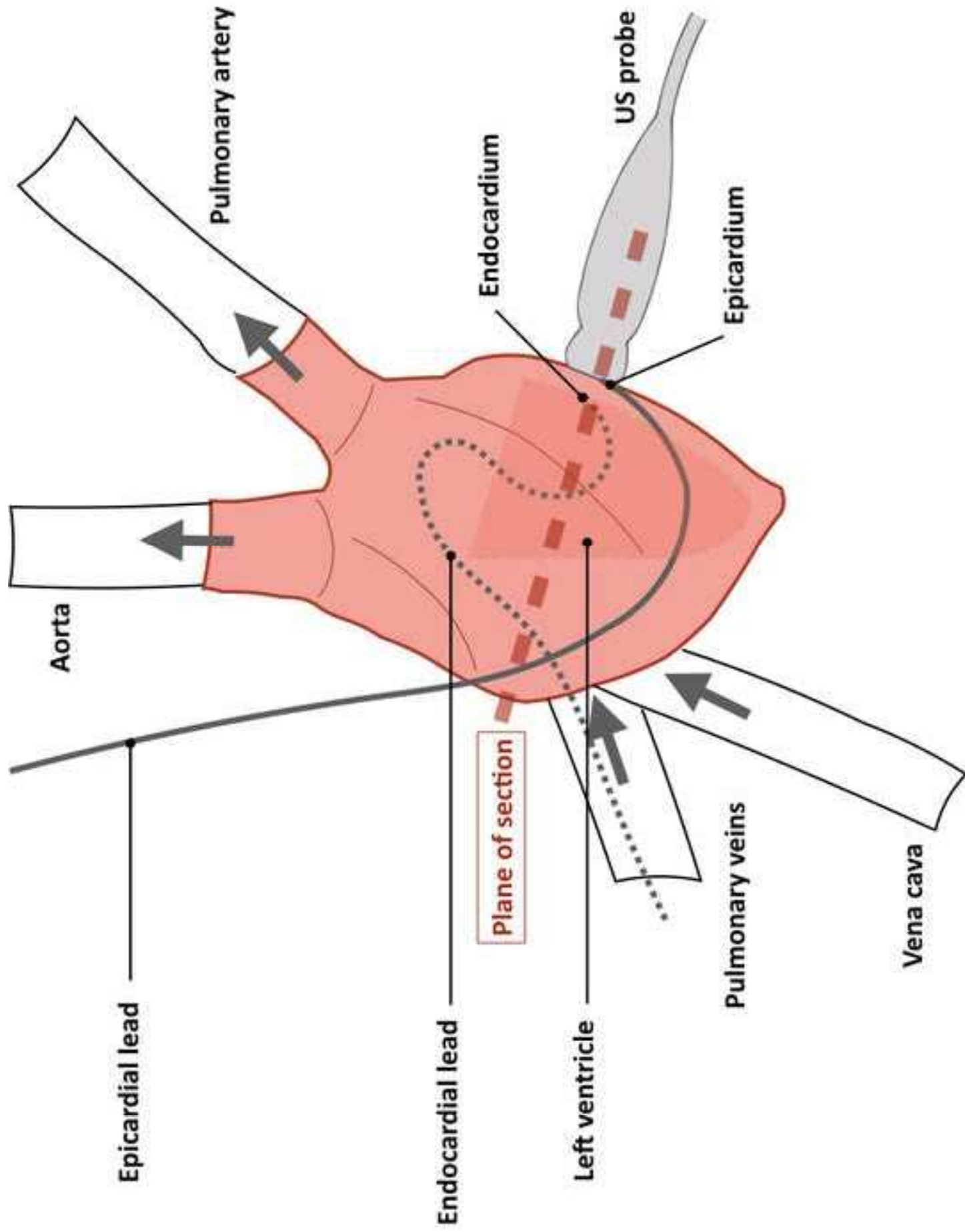
16

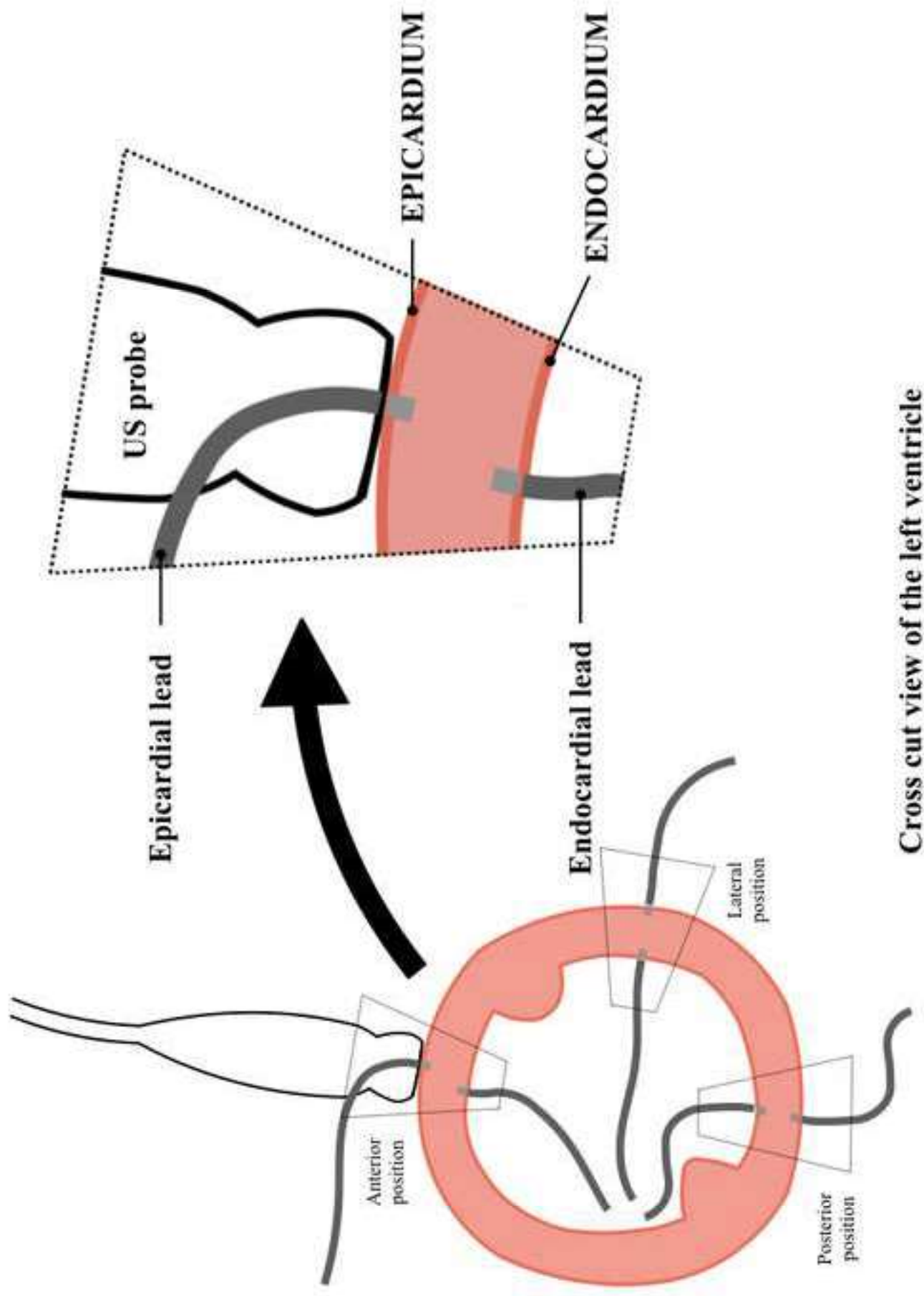
17 Figure 4: EWI during epicardial pacing. The first column shows the electrocardiogram: from
18 the first to the last line, a red dot depicts when the images were recorded at four different
19 moments of a cardiac cycle (ms). The second column shows the B-mode corresponding
20 images. The third column shows the corresponding EWI pictures (deformation depicted in
21 μm). The beginning of the induced electromechanical wave front is focal and clearly
22 distinguished on the upper right corner of the image (in red). It corresponds to the location of
23 the epicardial lead.

24

1 Figure 5: EWI during endocardial pacing. The first column shows the electrocardiogram:
2 from the first to the last line, a red dot depicts when the images were recorded at four different
3 moments of a cardiac cycle (ms). The second column shows the B-mode corresponding
4 images. The third column shows the corresponding EWI pictures (deformation depicted in
5 μm). The beginning of the induced electromechanical wave front is focal and clearly
6 distinguished on the lower left corner of the image (in red). It corresponds to the location of
7 the endocardial lead.

8





Cross cut view of the left ventricle

